Different elements, same results: time-resolved temperature determination by oxygen and nitrogen elements

Jinst

Published by IOP Publishing for Sissa Medialab

Received: *June 26, 2023*
Accepted: *July 7, 2023*
Published: *August 4, 2023*

Different elements, same results: time-resolved temperature determination by oxygen and nitrogen elements

S. Arjmand,[a,b,*] **M.P. Anania,**[b] **A. Biagioni,**[b] **M. Ferrario,**[b] **M. Galletti,**[b] **V. Lollo,**[b] **D. Pellegrini,**[b] **R. Pompili**[b] **and A. Zigler**[c]

[a] *Physics Department, Sapienza University of Rome, Piazzale Aldo Moro 5, Rome 00185, Italy*
[b] *INFN, Laboratori Nazionali di Frascati, Via Enrico Fermi 54, Frascati 00044, Italy*
[c] *Racah Institute of Physics, Hebrew University of Jerusalem, Edmond J. Safra Campus, Jerusalem 9190401, Israel*

E-mail: sahar.arjmand@lnf.infn.it

Abstract: The core purpose of this research is to use optical emission spectroscopy to determine the electron temperature (T_e) of a hydrogen plasma generated in a capillary discharge plasma, with a focus on its temporal variation. The plasma density (n_e) is first determined using the Stark broadening technique, which measures the broadening of spectral lines as a result of the electric field in the plasma. Subsequently, a passive spectroscopic technique is employed to estimate the electron plasma temperature by detecting the emitted light from the plasma. This spectral detection is performed using a visible range spectrometer. In this study, two elements, oxygen and nitrogen, are specifically selected based on the chemical composition of the capillary. The electron plasma temperature is estimated using the line ratio method, which involves comparing the intensities of two specific spectral lines emitted by the selected elements. By analyzing these line ratios, the electron plasma temperature can be inferred. The combination of the Stark broadening technique and line ratio method provides valuable insights into the plasma's physical characteristics, specifically its density and temperature.

Keywords: Plasma diagnostics - charged-particle spectroscopy; Plasma diagnostics - interferometry, spectroscopy and imaging; Wake-field acceleration (laser-driven, electron-driven)

*Corresponding author.

https://doi.org/10.1088/1748-0221/18/08/P08003

2023 JINST 18 P08003

Contents

2023 JINST 18 P08003

1 Introduction

Due to the possibility of using accelerators to create a compact high-energy particle by laser or particle wakefield acceleration (LWFA or PWFA), substantial research on this topic has been done recently [1–3]. A capillary discharge plasma can be used in the acceleration research domain to boost the acceleration gradients to reach higher acceleration energies. Specifically, electrons can be accelerated to giga-electron-volt (GeV) energies in the wake of a propagating laser pulse by a relativistic plasma wave oscillation, which is excited by the ponderomotive force of the intense laser pulse [4, 5]. Therefore, the LWFA/PWFA techniques used in gas-filled capillary equipment provide a sufficiently extended interaction between the laser/particle bunch and the accelerated electrons via plasma medium. Understanding the characteristics of the plasma is crucial before coupling the bunch's properties with the capillary plasma. Since the optical guiding of the laser/particle bunch in the plasma channel is extremely sensitive to the evolution of the transverse electron density profile, the temporal dynamics of the plasma density relative to its temperature is the fundamental factor in the characterization of a capillary plasma. Thus, to successfully generate high-energy electrons, precise plasma density and temperature measurements must be conducted.

2 Experimental section

The work described is part of the European project EuPRAXIA, which focuses on plasma-based accelerators and is being carried out at the SPARC_LAB test facility located at INFN-LNF in Frascati [6]. The experimental setup involves a capillary discharge plasma system, as shown in figure 1. A capillary made of VeroClear RGD810 is placed in a vacuum chamber that is evacuated to a pressure below 10^{-8} mbar. Hydrogen gas is then introduced into the capillary through two inlets, at a pressure ranging from 10 to 50 mbar. The capillary has a length of 3 cm and a diameter of 1 mm. A DC high-voltage power supply with a charging voltage of 12 kV is used to charge the capacitors, which in turn induces a plasma current of 400 A during the discharge. The high voltage difference between the two copper electrodes located at the capillary extremities is used to generate the discharge current. The current profile is acquired using an oscilloscope. During plasma discharge, the optical path collects the plasma emission, which is then directed towards a spectrometer. In this experiment, two separate spectrometers were utilized to capture and analyze different atomic lines. Each spectrometer was specifically chosen to target and measure specific atomic emissions. The SpectraPro275 is used to capture narrow atomic lines, while the iHR320 is

used to capture even narrower atomic lines. The SpectraPro 275 has a focal length of 275 mm and an aperture ratio of f/3.8, a grating with a groove density of 1200 g/mm, and a spectral resolution of 0.1 nm, while the iHR320 has a focal length of 320 mm, with an aperture ratio of f/4.1, a grating with a groove density of 600 g/mm, and a spectral resolution of 0.06 nm. The act of capturing images involves the usage of a camera that possesses fast-gating capabilities. In this particular case, the camera utilized is the Andor IStar 720 model, which has a resolution of 1024×255 pixels. We have conducted two in-situ calibrations, one for the x-axis and another for the y-axis. The y-axis calibration involves the 255-row pixels, which correspond to the capillary length. This axis provides information about the plasma density, depending on whether the plasma light is recorded longitudinally or from a transverse coordinate. Using copper electrodes that are 1 mm thick and positioned at the end of the capillary, a calibration process is performed on the 255-row pixel arrangement. The 1024-column pixels are used for the x-axis calibration, which provides spectral information for each line. We obtain the x-axis or wavelength calibration using a Hg-Ar lamp, which emits very sharp peaks. To synchronize all sections of plasma formation, we used a digital delay generator (Stanford Research DG535) to trigger signals in a single-shot manner. This external synchronization ensured that all components of the plasma were activated simultaneously.

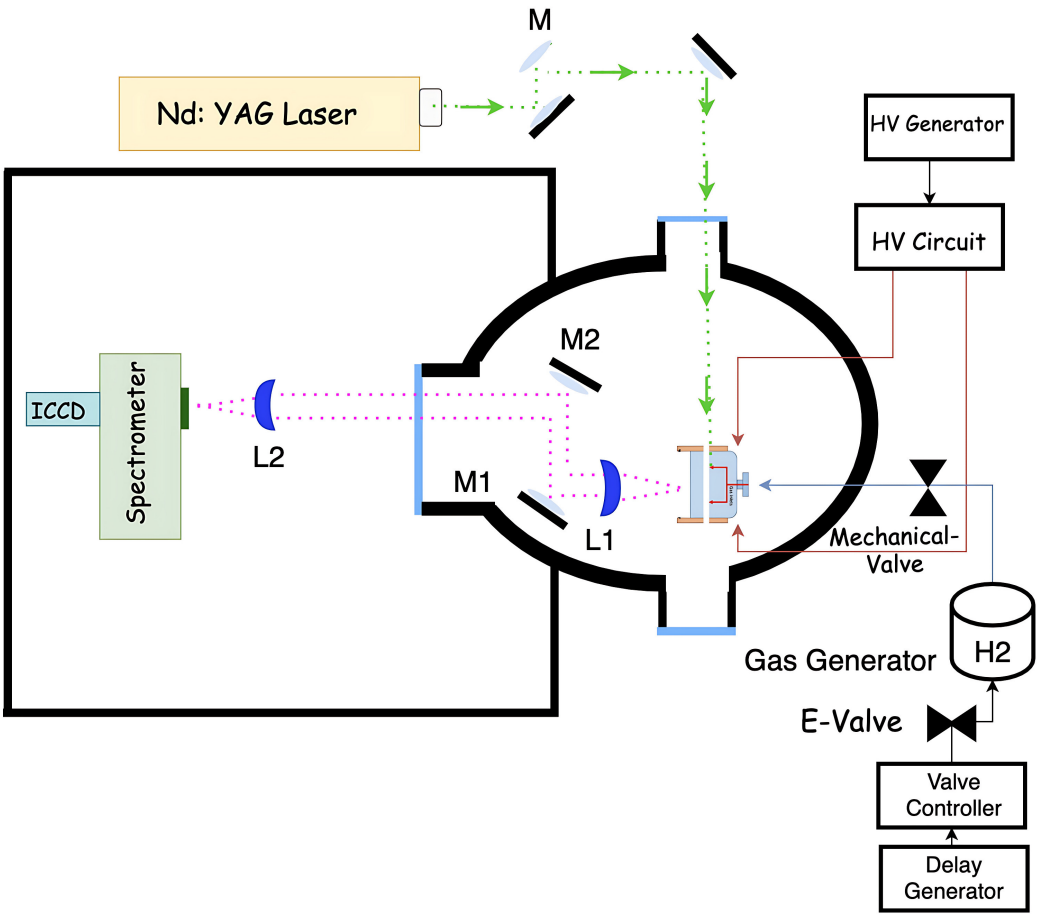

Figure 1. Experimental schematic of the plasma system used at the SPARC_LAB to form and characterize plasma inside a capillary discharge plasma.

2023 JINST 18 P08003

3 Electronic plasma density determination

Optical emission spectroscopy (OES) is a widely used diagnostic technique for measuring the emitted spectra from plasma, which contain information about the excited states of ions and atoms. OES employs the phenomenon of spectral line broadening (SLB) to analyse the emitted spectrum from a plasma, which is affected by the electronic density, n_e (cm^{-3}), and electronic temperature, T_e (eV), and can yield valuable information for characterizing the plasma properties. OES allows for non-invasive measurements of plasma parameters without disturbing the plasma, making it a preferred technique for plasma diagnostics. By analysing the emitted spectrum, information about the electronic density, electronic temperature, and other plasma properties can be obtained, providing insights into the behavior and characteristics of the plasma. The choice of plasma model can affect the techniques used for measuring plasma parameters. Various plasma models, such as the collisional radiative (CR), local thermodynamic equilibrium (LTE), steady-state Corona, and time-dependent Corona models, are relevant to different electron interaction mechanisms [7]. In our case, an LTE condition has been assumed, which implies that the populations of different atomic states are in thermal equilibrium with the electron temperature. There are various methods to determine the electron temperature of a plasma, and one of the most direct ways is to use spectral line intensities [7]. Spectral line intensities can provide valuable information about the temperature dynamics of a plasma by measuring the relative intensities of spectral lines emitted by different ions. The temperature determination equations for spectroscopic techniques compare the ratios of spectral line intensities from different ionization stages of a particular element and use the natural logarithm function (ln) to determine the temperature. The line ratio method involves calculating the natural logarithm of the ratio of the intensities of two spectral lines from different ionization stages of the same element, denoted as I_1 and I_2, respectively. The general formula for the line ratio method is,

$$T = \frac{b}{\ln\left(\frac{I_1}{I_2}\right)}, \tag{3.1}$$

where T is the temperature, b is a constant that varies depending on the specific set of lines and the ionization balance of the element, I_2 is the intensity of the higher ionization line, and I_1 is the intensity of the lower ionization line. The ionization potential of an element depends on its electron configuration. As the temperature of a plasma increases, the electrons in the atoms are excited to higher energy levels, and some of them become ionized. The relative populations of different ionization stages of an element in a plasma can be determined from the intensity ratios of their spectral lines. The intensity of a spectral line depends on the number of atoms in the plasma that emit that line, which in turn depends on the population of the corresponding ionization stage. The ratio of the intensities of two spectral lines from different ionization stages of the same element is related to the ratio of the populations of those ionization stages. In this study, the technique of relative line intensities of spectral lines with subsequent ionization stages is proposed to analyze the time-resolved temperature behavior of oxygen and nitrogen elements in a hydrogen plasma. However, it is essential to assume that the plasma is in local thermal equilibrium (LTE) to determine the electronic temperature by employing the relative intensities between two spectral lines. By examining the spectral line intensities of subsequent ionization states in combination with knowledge of electron plasma densities, the electron temperature of a plasma can be determined.

2023 JINST 18 P08003

Reference [8] provides further information on the relationship associated with the Saha-Boltzmann equation:

$$R = \frac{I_2}{I_1} = \frac{\lambda_1^3 f_{(2)} g_2}{\lambda_2^3 f_{(1)} g_1} \left(4\pi^{\left(\frac{3}{2}\right)} a_0^3 n_e\right)^{(-1)} \left(\frac{T_e}{E_H}\right)^{\left(\frac{3}{2}\right)} \times \exp\left(-\frac{E_2 + E_\infty - E_1 - \Delta E_\infty}{T_e}\right). \tag{3.2}$$

Indeed, the intensity ratio depends on the physical properties of the plasma such as electron density, electron temperature, and the energy levels of the atoms or ions. This formula allows for the calculation of these properties by comparing the measured intensity ratio to the expected value based on the known properties of the plasma and the atomic or ionic species being studied. However, the relationship between the parameters in the formula is not straightforward and non-linear, and understanding their individual effects requires a detailed understanding of their atomic process and data. In this context, the parameters I_1 and I_2 (A U) are the intensities of two spectral lines, f_1 and f_2 (DI) are the absorption oscillator strength of two spectral lines, λ_1 and λ_2 (nm) are the spectral lines wavelength, g_1 and g_2 are the statistical weights (degeneracy) of two spectral lines, E_1 and E_2 (eV) are the transition energies of the producing two spectral lines. The parameters E_∞ (eV), E_H (eV), and a_0 (m) are the ionization energy of the atom with the lower ionization stage, Bohr radius, and hydrogen ionization energy, respectively. Indeed, the oscillator strength is a measure of the probability of an emission or absorption transition of electromagnetic radiation and Bohr radius is an estimate of the most likely distance between the nucleus and the electron in a hydrogen atom's ground state:

$$a_0\,[\mathrm{m}] = \frac{4\pi\varepsilon_0\hbar^2}{m_e e^2}, \tag{3.3}$$

where ε_0 (F m^{-1}) is the vacuum permittivity, $\hbar$ (J s) is the reduced Planck constant, m_e (kg) is the electron mass, and e (C) is the elementary charge. The statistical weights are obtained from the appropriate total angular momentum quantum of the state ($g_{1,2} = 2J+1$). In the presence of plasma, the ionization energy of an atom can be altered due to interactions with other charged particles. To account for these interactions and the resulting changes in the ionization energy of the lower ionization stage, the parameter ΔE_∞ (eV) is introduced as a correction factor. The parameter ΔE_∞ is the correction factor to the ionization energy of the lower ionization stage [8],

$$\Delta E_\infty\,[\mathrm{eV}] = 3Z\frac{e^2}{4\pi\varepsilon_0}\left(\frac{4\pi n_e}{3}\right)^{\frac{1}{3}}. \tag{3.4}$$

The symbol Z denotes the number of electrons that are lost by the atom at the lower ionization stage. The corresponding correction factor was measured for the plasma density at various time points after gas breakdown (as shown in figure 2). In an LTE system, the estimation of electron density can be achieved using a passive spectroscopic technique called Stark broadening of a spectral line. Stark broadening occurs due to the interaction between the emitting atom and the electric field generated by charged particles present in the plasma at the emission location. This dependence on the density of charged particles implies that in the case of singly charged ionized plasma, the electron density (n_e) is equal to the ion density (n_i). The expression for electron density takes into account the effects of quasi-static ion broadening and impact-electron broadening, derived from the theory of Stark broadening. Consequently, it is possible to extract the electron plasma density using

2023 JINST 18 P08003

the following formula, which relates the full width at half maximum (FWHM) of Balmer beta (H_β) to the electronic plasma density based on a SLB diagnostic [9–13]:

$$n_e = 8.02 \times 10^{12} \left(\frac{\Delta\lambda_S}{\alpha_{1/2}} \right)^{\frac{3}{2}} \text{cm}^{-3}. \tag{3.5}$$

Here, $\Delta\lambda_{\frac{1}{2}}$ is the Stark broadened FWHM line width, n_e is the electronic plasma density, $\alpha_{1/2}$ is the reduced wavelength, which is a function of plasma density and temperature, and literately tabulated [14]. This coefficient for the H_β line ranges between line ranges between 8.51×10^{-2} Ångstrom and 9.27×10^{-2} Ångstrom at a plasma density of $10^{17}\,\text{cm}^{-3}$ and a temperature of 1–4 eV [7]. The FWHM is calculated from the Lorentzian fit of the H_β spectral line profiles [15]. Hence, once the electron density is determined, the correction factor is calculated as a function of plasma recombination time. Figure 2 illustrates both the plasma density and the correction factor for the time range of 1000 to 2000 ns following the gas breakdown. The average values presented are based on 50 separate measurements of plasma density profiles, with a gate width of 100 ns. The time-resolved plasma density is achievable by varying the relative delay time between the discharge triggering and data acquisition time.

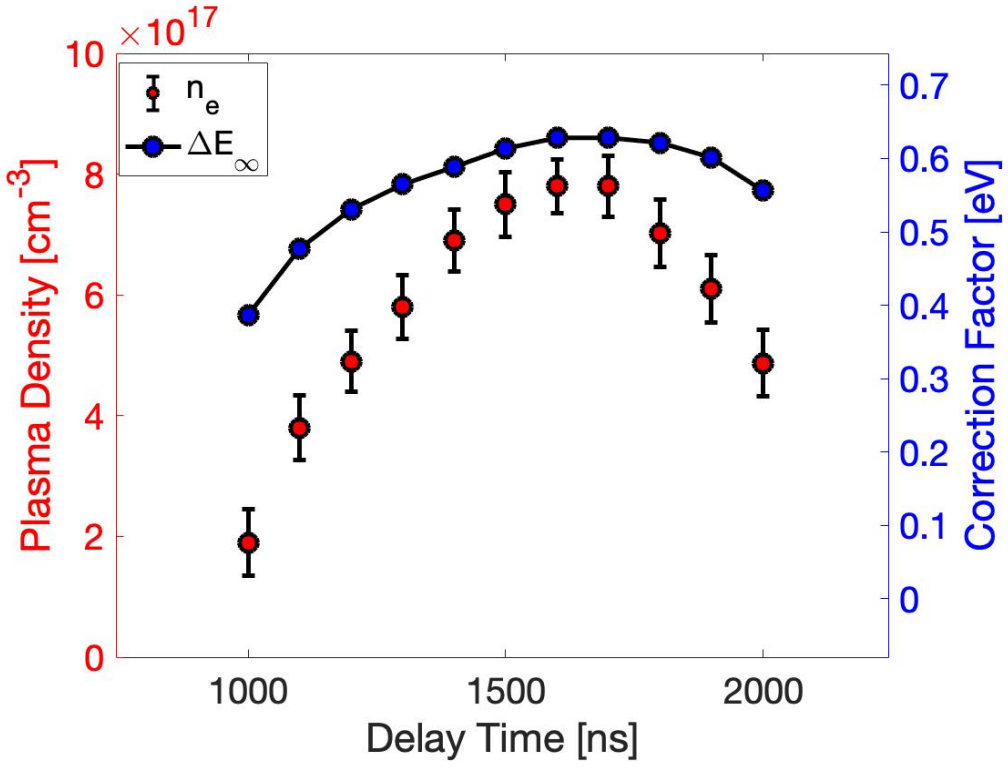

Figure 2. Retrived experimental plasma density from H_β line and correction factor for delay times ranging from 1000 to 2000 ns in a 3 cm length, 1 mm diameter with double-inlet capillary discharge plasma.

The atomic lines of oxygen (16.50%), nitrogen (0.57%), and carbon (82.92%) can be detected in the chemical composition of our VeroClear RGD810 capillary. This suggests the potential production of ions with various ionization stages such as C I, C II, C III, O I, O II, O III, N I, N II,

2023 JINST 18 P08003

and N III in the wavelength range of 400–540 nm, assuming specific plasma density of 10^{17} cm^{-3} and temperature of 1–4 eV. However, experimental results have only detected ions of C I, C II, C III, O II, O III, N II, and N III. Figure 3 presents examples of the potential spectral lines of O, N, and C that may be emitted within the examined wavelength range, including the spectral lines considered for analysis. For the determination of the electron temperature, we specifically selected oxygen ions: O II at 471.9803 nm [from $(2s^2 2p^2(^3p)4s)$ to $(2s^2 2p^2(^3p)5p)$], and O III at 508.8922 nm [from $(2s^2 2p(^2p^\circ)4d)$ to $(2s2p^2(^4p)3d)$]; and nitrogen ions: N II at 471.8377 nm [from $(2s2p^2(^4p)3p)$ to $(2s2p^2(^4p)3d)$] and N III at 453.970 nm [from $(2s^2 4p)$ to $(2s^2 5s)$], for measurements. The selection of these particular spectral lines was based on their notable differences in intensity when compared to each other, while also exhibiting minimal variations in wavelength in comparison to the NIST database.

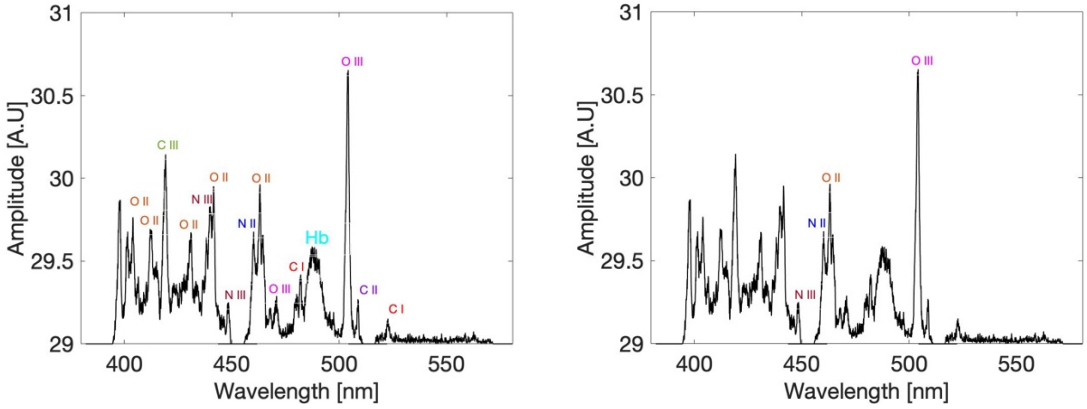

Figure 3. An example of emitted spectral lines of carbon, nitrogen, and oxygen elements (left) and the considered spectral lines (right) all within the visible range.

Using distinct elements, such as oxygen and nitrogen, in a time-resolved temperature analysis in plasma research can provide several benefits. Different species behave differently in a plasma environment due to their unique ionization energies, excitation energies, and other atomic properties. By utilizing different elements, we can obtain species-specific temperature information, which allows for a more detailed understanding of the behavior of individual elements in the plasma. Using different elements in a time-resolved temperature analysis can provide robustness to the results obtained. If similar temperature behaviors are observed for different elements, it can enhance the confidence in the findings and conclusions of the study.

Additionally, using multiple elements can help identify any element-specific effects or anomalies in the plasma behavior. To investigate the time-resolved temperature behavior, we monitored the changes in the relative line intensities of spectral lines emitted by oxygen and nitrogen species. The temporal behavior of the plasma temperature will be analyzed by tracking the changes in the relative line intensities of spectral lines associated with different ionization stages of oxygen and nitrogen species. Figure 4 displays the relative intensity of spectral lines corresponding to the oxygen and nitrogen elements at different times during this recombination process. The changes in the intensity of these lines over time can provide insights into how the elements behave within the plasma, such as how they combine and interact with other particles or how they contribute to the overall behavior of the plasma.

2023 JINST 18 P08003

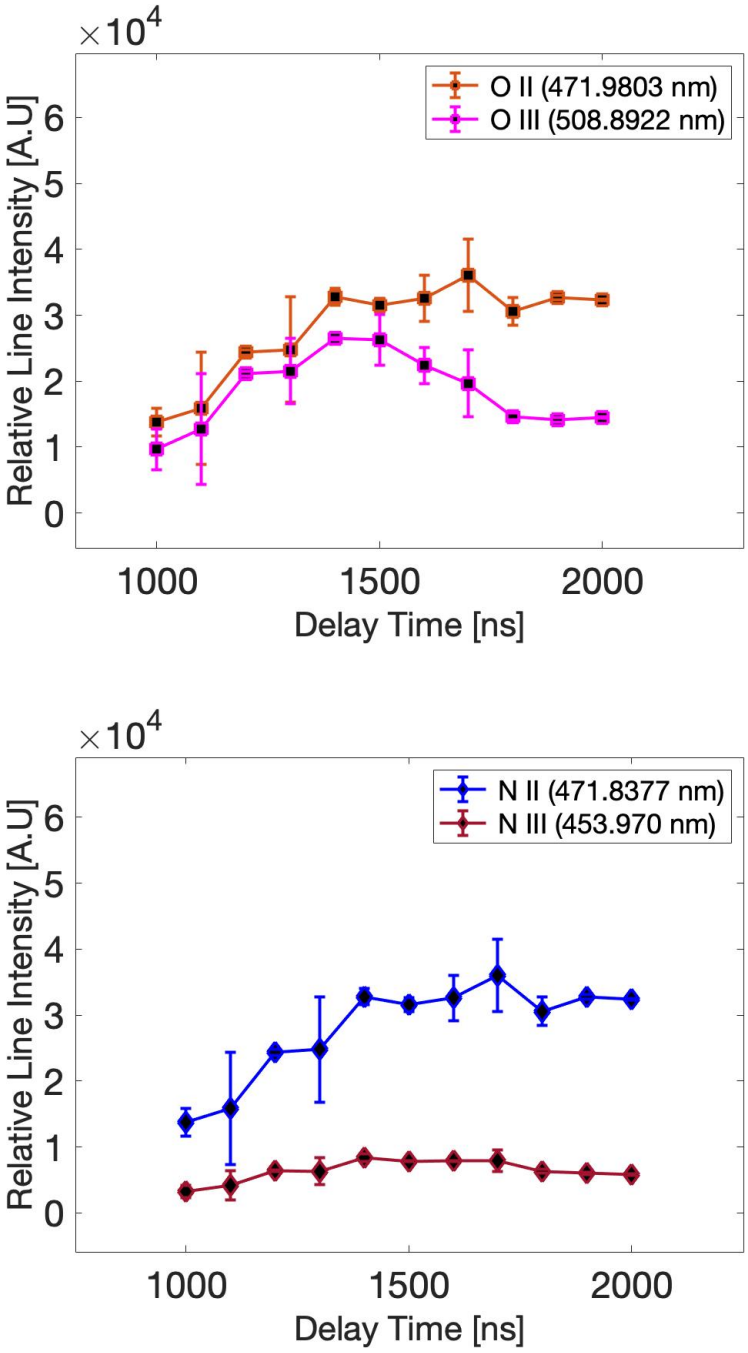

Figure 4. Relative intensity evolution of the lines at different delay times ranging from 1000 to 2000 ns: relative intensity of oxygen ions (top) and nitrogen ions (bottom).

Table 1 is reported the physical constants and spectroscopic data for the considered spectral lines. The physical constants and spectroscopic data for these spectral lines were collected from the National Institute of Standards and Technology (NIST) database and Griem spectroscopy literature, as referenced in [8, 16]. The electron temperature can be computed using eq. (3.2) by inputting the appropriate spectroscopic data for the elements of interest from table 1.

2023 JINST 18 P08003

Table 1. Physical constant and spectral data of the oxygen and nitrogen ions.

Oxygen Element Spectroscopic Data	
Parameter	**Value**
λ_1: Wavelength of O II	471.9803 (nm)
λ_2: Wavelength of O III	508.492 (nm)
g_1: Statistical Weight of O II	1
g_2: Statistical Weight of O III	1
f_1: Oscillator Strength of O II	8.57×10^4 (DI)
f_2: Oscillator Strength of O III	6.15×10^6 (DI)
J_1: Lower-level and Upper-level Angular Momentum Quantum Number of O II	$\frac{3}{2}$, $\frac{3}{2}$
J_2: Lower-level and Upper-level Angular Momentum Quantum Number of O III	2, 2
E_1: Excitation Energy of O II	2.62 (eV)
E_2: Excitation Energy of O III	2.43 (eV)
E_∞: Ionization Energy of Lower State of O II	35.11730 (eV)
Z: Number of Electrons Lost by O II	1
Nitrogen Element Spectroscopic Data	
Parameter	**Value**
λ_1: Wavelength of N II	471.8377 (nm)
λ_2: Wavelength of N III	453.970 (nm)
g_1: Statistical Weight of N II	1
g_2: Statistical Weight of N III	1
f_1: Oscillator Strength of N II	3.02×10^7 (DI)
f_2: Oscillator Strength of N III	5.71×10^7 (DI)
J_1: Lower-level and Upper-level Angular Momentum Quantum Number of N II	4, 4
J_2: Lower-level and Upper-level Angular Momentum Quantum Number of N III	$\frac{1}{2}$, $\frac{1}{2}$
E_1: Excitation Energy of N II	2.62 (eV)
E_2: Excitation Energy of N III	2.77 (eV)
E_∞: Ionization Energy of Lower State of N II	29.6013 (eV)
Z: Number of Electrons Lost by N II	1
Physical Constants	
Parameter	**Value**
E_H: Hydrogen Ionization Energy	13.6 (eV)
ε_0: Vacuum Permittivity	8.85×10^{-12} (F m^{-1})
a_0: Bohr Radius	$5.2917724 \times 10^{-11}$ (m)
m_e: Electron Mass	9.10938×10^{-31} (kg)
e: Electron Charge	1.602×10^{-19} (C)
$\hbar$: Reduced Planck Constant	1.05457×10^{-34} (J s)

2023 JINST 18 P08003

4 Findings and analysis

The results, presented in figure 5, demonstrate similar temperature trends for both elements within the time range of 1000 to 2000 ns after the discharge breakdown. In the case of oxygen ions, the temperature starts at the lowest observed value of 2.15 eV and gradually increases, reaching a peak of 2.34 eV. It then stabilizes around 2.22 eV. Conversely, the temperature evolution for nitrogen ions begins at a slightly lower value of 2.09 eV compared to oxygen ions, reaches its maximum of 2.33 eV, and then gradually decreases to 2.23 eV. These results indicate that both oxygen and nitrogen ions exhibit similar temperature trends during the studied time frame, with variations in their initial and maximum temperature values. The findings provide insights into the behavior of electronic plasma temperature for these elements after gas breakdown and offer valuable information for understanding the plasma dynamics and processes involved in the system under investigation.

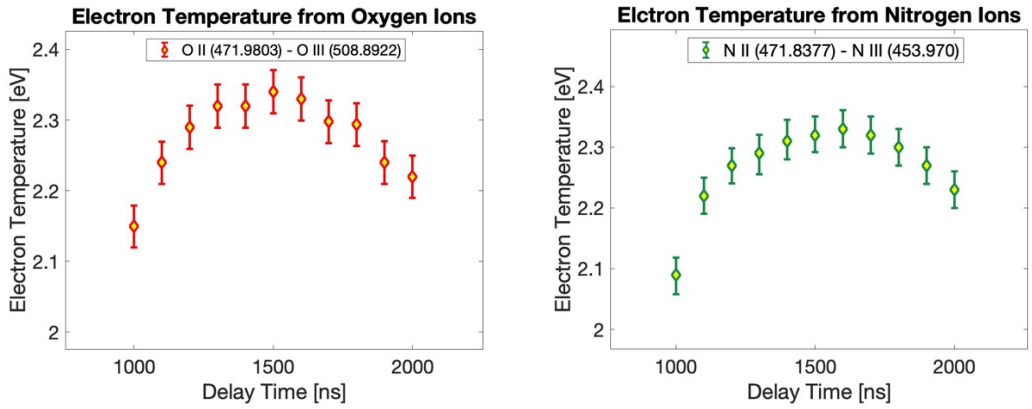

Figure 5. Electron plasma temperature (T_e) from oxygen element (left) and from nitrogen element (right) as a function time after gas breakdown.

Figure 6 illustrates a comparison of the electron plasma temperatures for nitrogen and oxygen ions as a function of time, measured in nanoseconds, after the gas breakdown. It is evident from the result that the temperatures of both elements exhibit slight fluctuations over time after the breakdown of the gas, with some overlapping at certain delay times. These measurements indicate that the plasma temperature remains relatively low, around 2 eV, for both nitrogen and oxygen ions. The variations in temperature with respect to time can be explained by different factors, including the amount of energy being supplied to the plasma, the plasma density, and the specific conditions of the gas breakdown experiment. These factors have the potential to impact the energy exchange mechanisms between the free electrons and other particles in the plasma, which can result in alterations in the electronic plasma temperature. The overlapping of the temperatures of nitrogen and oxygen ions at certain delay times suggests that they may have similar energy characteristics under the given experimental conditions.

In figure 7, a simulation is presented that showcases the complete range of spectral lines (O II, O III, N II, and N III) spanning from 450 to 540 nm [17]. The figure displays both the individual spectral lines (figure 7(a)–7(d)) and their cumulative sum (figure 7(e)). The simulation is based on an electron plasma density of 6.8×10^{17} cm^{-3}, a temperature of 2.32 eV, and a delay period of 1500 ns.

2023 JINST 18 P08003

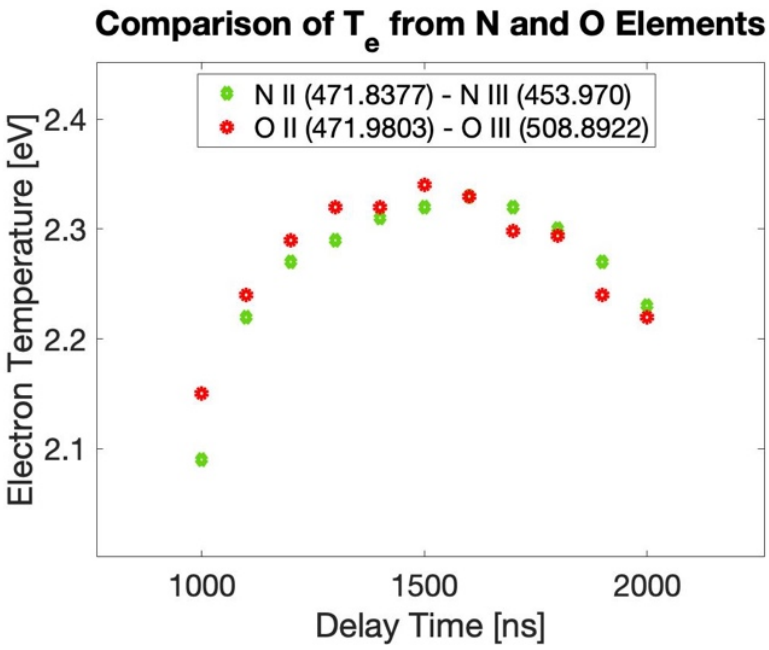

Figure 6. A comparison of electron plasma temperature in a 3 cm long, 1 mm diameter capillary from oxygen (red points) and nitrogen (green points) elements.

Given the capillary's chemical composition, with carbon accounting for 82.92%, oxygen for 16.50%, and nitrogen for 0.57%, the simulation demonstrates conformity to the expected presence of nitrogen and oxygen elements. The simulation conducted for the given mixture of spectrum, along with the specified plasma density and plasma temperature at delay 1500 ns, reveals that a total of 365 lines will be present. Despite variations in the intensities of the ions (O II, O III, N II, and N III) observed in the experimental results, their use enabled the estimation of the electron plasma temperature to be approximately 2 eV, in line with expectations. The comparison between experimental and theoretical results demonstrates reasonable agreement, validating the chosen method. Thus, the plasma electron temperature can be reliably estimated as approximately 2 eV using the spectral lines emitted by oxygen ions (O II and O III) and nitrogen ions (N II and N III).

2023 JINST 18 P08003

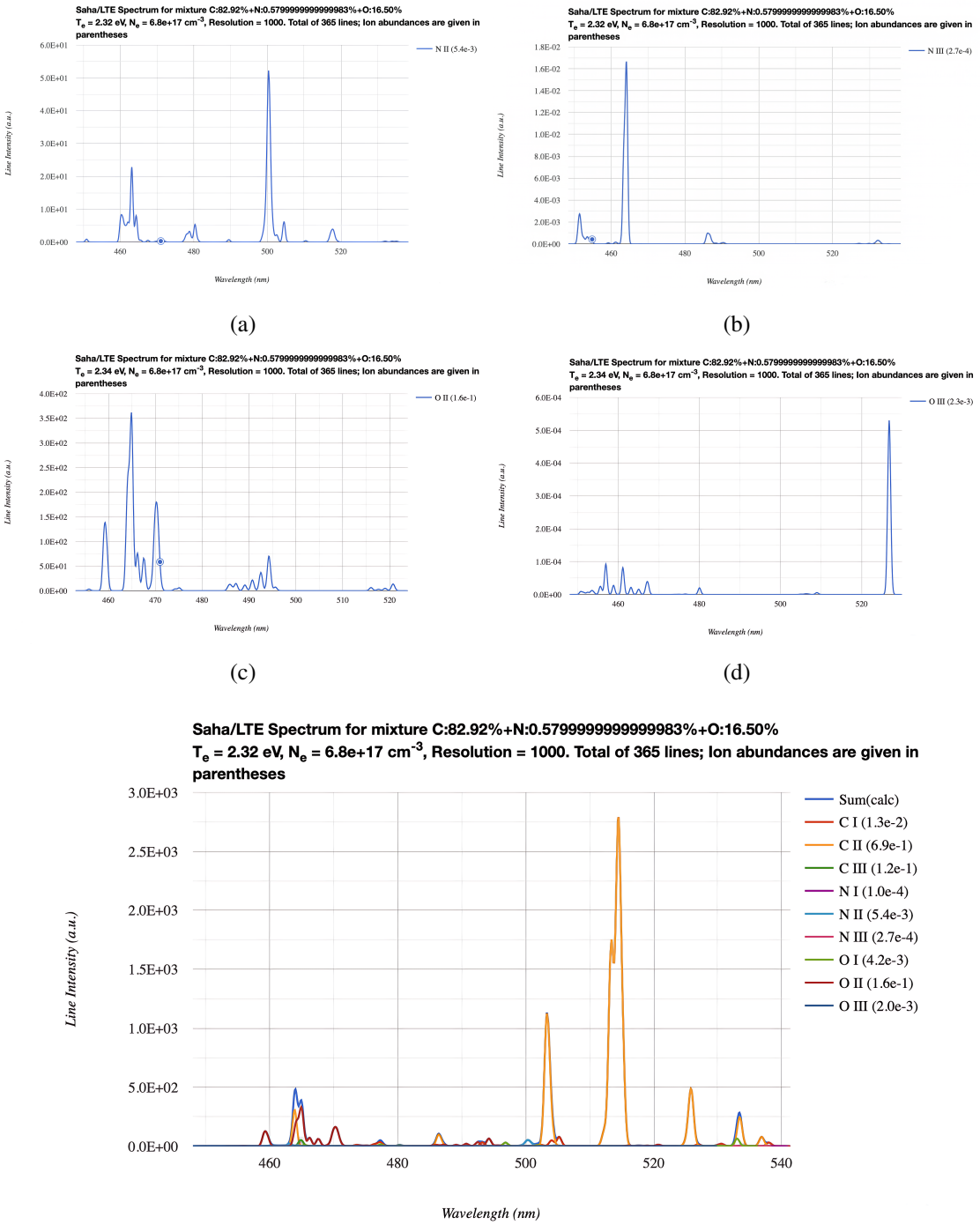

Figure 7. An illustration of the anticipated spectral lines of O II (a), O III (b), N II (c), N III (d), and the combined sum of all spectral lines (e) inside a 3 cm length, 1-mm diameter capillary with the electron plasma temperature of 2.32 eV and density of 6.8×10^{17} cm^{-3} at a delay time of 1500 ns.

2023 JINST 18 P08003

5 Conclusions

The primary motivation of this work is to describe the plasma's physical characteristics (n_e, T_e). Two plasma diagnostics were employed to characterize the plasma in the hydrogen-filled capillary discharge, namely the spectral line broadening induced by the Stark effect and the relative intensities of subsequent ionization stages of the same element. The plasma density (n_e) was determined primarily through the Stark broadening, while the electron temperature (T_e) was obtained using the two-line intensity method. The main objective of this study was to experimentally measure the plasma temperature and compare it with theoretical results. Previous studies on discharge capillaries and spectral line broadening commonly estimated the plasma temperature to be approximately 1–4 eV. In this study, we aim to improve the accuracy of temperature measurement by allowing it to evolve naturally over time, thereby eliminating the need for ad hoc guesswork based on incomplete or uncertain information. This results in a more precise and reliable measurement of temperature. In summary, it can be stated that there is a valid agreement between the experimental results and the theoretical predictions obtained from the simulations. A reasonable correlation between the theoretical data and experimental observation is defined by comparing their results. Therefore, the two lines' intensity method with different ionization stage can be used successfully to determine the electron temperature in a variety of low-pressure or temperature plasmas. We have found that the ratio of two lines' intensity method is one of the most convenient in such measurements. In summary, using different elements in a time-resolved temperature analysis in plasma provided us cross-validation and confirmation of the reliability and accuracy of the technique used. The consistency in temperature results from oxygen and nitrogen elements can suggest that the plasma is in a state of thermodynamic equilibrium. When the plasma is in thermodynamic equilibrium, the populations of different atomic states are in thermal equilibrium with the electron temperature, and the temperature analysis results from different species should be consistent. This can provide insights into the equilibrium behavior of the plasma and help validate assumptions of local thermal equilibrium made in the analysis.

Acknowledgments

This research activity has partially been supported by the EU Commission in the Seventh Framework Program, Grant Agreement 312453-EuCARD-2, the European Union Horizon 2020 research, innovation program with the Grant Agreement No. 653782 (EuPRAXIA), and the INFN with the GRANT73/PLADIP grant.

References

[1] W.P. Leemans et al., *Multi-GeV Electron Beams from Capillary-Discharge-Guided Subpetawatt Laser Pulses in the Self-Trapping Regime*, *Phys. Rev. Lett.* **113** (2014) 245002.

[2] I. Blumenfeld et al., *Energy doubling of* 42 *GeV electrons in a metre-scale plasma wakefield accelerator*, *Nature* **445** (2007) 741.

[3] M. Litos et al., *High-efficiency acceleration of an electron beam in a plasma wakefield accelerator*, *Nature* **515** (2014) 92.

2023 JINST 18 P08003

[4] T. Tajima and J.M. Dawson, *Laser electron accelerator*, *Phys. Rev. Lett.* **43** (1979) 267.

[5] W.P. Leemans et al., *GeV electron beams from a cm-scale accelerator*, *Nat. Phys.* **2** (2006) 696.

[6] M. Ferrario et al., *EuPRAXIA@SPARC_LAB Design study towards a compact FEL facility at LNF*, *Nucl. Instrum. Meth. A* **909** (2018) 134 [arXiv:1801.08717].

[7] M. Hassouba et al., *A comparative spectroscopic study on emission characteristics of DC and RF discharge plasma using different gases*, *Life Sci. J.* **11** (2014) 9.

[8] H.R. Griem, *Plasma spectroscopy*, McGraw-Hill, New York, NY, U.S.A. (1964).

[9] D.G. Jang, M.S. Kim, I.H. Nam, H.S. Uhm and H. Suk, *Density evolution measurement of hydrogen plasma in capillary discharge by spectroscopy and interferometry methods*, *Appl. Phys. Lett.* **99** (2011) 141502.

[10] S. Arjmand et al., *Characterization of plasma sources for plasma-based accelerators*, 2020 *JINST* **15** C09055.

[11] S. Arjmand et al., *Spectral line shape for plasma electron density characterization in capillary tubes*, *J. Phys. Conf. Ser.* **2439** (2023) 012012.

[12] S. Arjmand et al., *Spectroscopic Measurements as Diagnostic Tool for Plasma-Filled Capillaries*, in proceedings of the *13th International Particle Accelerator Conference (IPAC 2022)*, Muangthong Thani, Thailand, 17–22 June 2022, *JACoW* **IPAC2022** (2022) WEPOST035.

[13] S. Arjmand et al., *Investigating of plasma diagnostics by utilizing spectroscopic measurements of Balmer emission*, 2023 *JINST* **18** C05007.

[14] H.R. Griem, *Spectral line broadening by plasmas*, Academic Press, Amsterdam, The Netherlands (1974).

[15] C.G. Parigger, K. Drake, C. Helstern and G. Gautam, *Laboratory Hydrogen-Beta Emission Spectroscopy for Analysis of Astrophysical White Dwarf Spectra*, *Atoms* **6** (2018) 36.

[16] NIST ASD Team, *Atomic Spectra Database*, version 5.9 (2021).

[17] A. Kramida, K. Olsen and Y. Ralchenko, *NIST LIBS Database*, https://physics.nist.gov/PhysRefData/ASD/LIBS/libs-form.html.

2023 JINST 18 P08003